THE JOURNAL OF PHYSICAL CHEMISTRY B

Article

pubs.acs.org/JPCB

Nuclear Hyperfine and Quadrupole Tensor Characterization of the Nitrogen Hydrogen Bond Donors to the Semiquinone of the Q_B Site in Bacterial Reaction Centers: A Combined X- and S-Band $^{14,15}N$ ESEEM and DFT Study

Alexander T. Taguchi,[†] Patrick J. O'Malley,*[,∥] Colin A. Wraight,*[,‡] and Sergei A. Dikanov*[,§]

[†]Center for Biophysics and Computational Biology, [‡]Department of Biochemistry, [§]Department of Veterinary Clinical Medicine, University of Illinois at Urbana−Champaign, Urbana, Illinois 61801, United States

[∥]School of Chemistry, The University of Manchester, Manchester M13 9PL, U.K.

Supporting Information

ABSTRACT: The secondary quinone anion radical Q_B^- (SQ_B) in reaction centers of *Rhodobacter sphaeroides* interacts with N_δ of His-L190 and N_p (peptide nitrogen) of Gly-L225 involved in hydrogen bonds to the Q_B carbonyls. In this work, S-band (~3.6 GHz) ESEEM was used with the aim of obtaining a complete characterization of the nuclear quadrupole interaction (nqi) tensors for both nitrogens by approaching the cancelation condition between the isotropic hyperfine coupling and ^{14}N Zeeman frequency at lower microwave frequencies than traditional X-band (9.5 GHz). By performing measurements at S-band, we found a dominating contribution of N_δ in the form of a zero-field nqi triplet at 0.55, 0.92, and 1.47 MHz, defining the quadrupole coupling constant $K = e^2qQ/4h = 0.4$ MHz and associated asymmetry parameter $\eta = 0.69$. Estimates of the hyperfine interaction (hfi) tensors for N_δ and N_p were obtained from simulations of 1D and 2D $^{14,15}N$ X-band and three-pulse ^{14}N S-band spectra with all nuclear tensors defined in the SQ_B g-tensor coordinate system. From simulations, we conclude that the contribution of N_p to the S-band spectrum is suppressed by its strong nqi and weak isotropic hfi comparable to the level of hyperfine anisotropy, despite the near-cancelation condition for N_p at S-band. The excellent agreement between our EPR simulations and DFT calculations of the nitrogen hfi and nqi tensors to SQ_B is promising for the future application of powder ESEEM to full tensor characterizations.

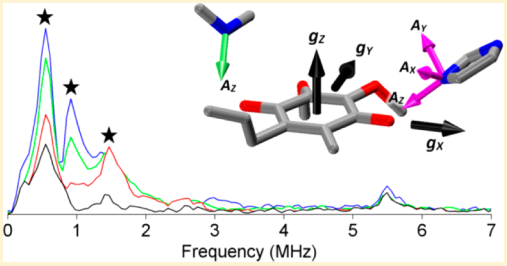

INTRODUCTION

Quinones are ubiquitous and versatile redox mediators in biological energy conversion systems. Their versatility stems from the ability to tune their redox properties over a very wide range, achieved by interactions with the protein environment of the quinone binding site. However, in no case is the nature of these interactions fully characterized or understood. The bacterial photosynthetic reaction center (RC), with two quinones, Q_A and Q_B, has proven to be an exceptional model for studying the underlying structure−function relationships.

In RCs from *Rhodobacter (Rb.) sphaeroides*, the quinones acting as Q_A and Q_B are both identical ubiquinone-10 molecules but exhibit very different functionalities.[1−3] The primary acceptor Q_A is a tightly bound prosthetic group, while the secondary quinone Q_B serves as a mobile carrier of two reducing equivalents. The properties of the two quinones are largely determined by the protein environments of the two quinone sites.[3−5] Existing RC crystal structures show significant uncertainty in the conformations of the two quinones, and especially a wide variability of the Q_B binding.[5] There are several different proposed orientations of Q_B, including binding in a location distal from a central Fe^{II}−$(His)_4$ complex.[6,7] However, the proximal binding of Q_B seen in earlier structures is also that seen in illuminated crystal structures, which likely traps the semiquinone state (SQ_B) in the active position.[6,7] The potential hydrogen bond donors to Q_B include the four residues His-L190, Ser-L223, Ile-L224, and Gly-L225, inferred from X-ray structures.

An alternative way to characterize the SQ state in proteins is through EPR, exploiting its paramagnetism.[8,9] EPR measures the interaction between the electron spin of the SQ and the nearby magnetic nuclei (^1H, ^{13}C, ^{14}N or ^{15}N, ^{17}O) of the quinone and protein. Using high-resolution pulsed EPR techniques (ENDOR, ESEEM), detailed information on the O···H···N hydrogen bonds can be obtained. This includes the ^1H and $^{14(15)}N$ hfi tensors (which depend on the geometry of the H-bonds and the spin density distribution over the SQ and H-bonds) and the ^{14}N nqi tensors (which reflect the chemical type of the coupled nitrogen, and the population and configuration of its electronic orbitals). X-band (~9.7 GHz) ^{14}N and ^{15}N 2D ESEEM spectra clearly show the interaction of

Received: November 8, 2013
Revised: January 14, 2014
Published: January 17, 2014

two nitrogens with SQ_B, each carrying transferred unpaired spin density.[10] Quadrupole coupling constants estimated from the ^{14}N spectra indicate them to be a protonated nitrogen of an imidazole residue and an amide nitrogen of a peptide group. The imidazole nitrogen (isotropic coupling $a(^{14}N)$ = 1.5 MHz) can only be assigned to N_δ of His-L190, consistent with existing X-ray structures. The second nitrogen ($a(^{14}N)$ = 0.5 MHz) could not be specified between two candidates (Ile-L224 and Gly-L225), and selective ^{15}N isotope labeling is needed for unambiguous assignment of this nitrogen. However, computational work assigned the $a(^{14}N)$ = 0.5 MHz coupling to the peptide nitrogen (N_p) of Gly-L225.[11] The hfi coupling of other protein nitrogens with SQ_B was not resolved (<0.1 MHz), indicating that H-bonds with other nitrogens were much weaker or absent.

In our previous study,[10] the principal values of the hfi tensors and their directions relative to the g-tensor axes for the two H-bonded nitrogens were undetermined because simulations of ^{15}N 2D ESEEM spectra were performed separately for each nitrogen without a common coordinate system defining the principal axes for all nuclear tensors. Additionally, the principal values and directions of the nqi tensors of the two ^{14}N (with hfi couplings $|a(^{14}N)| \leq 1.5$ MHz) were not determined experimentally from the X-band spectra due to substantial deviations from the cancelation condition $|\nu_N - |a|/2| = 0$. This prevented the observation of the nuclear transitions with pure zero-field nqi frequencies that would provide the principal values of the nqi tensor. Performing the experiments at lower microwave frequencies and consequently a lower Zeeman frequency (ν_{14N}) should improve the fulfillment of the cancelation condition and allow for the observation of the zero-field nqi frequencies.

In this article, therefore, we present the results of an S-band (~3.6 GHz) ^{14}N ESEEM study of SQ_B and its analysis in conjunction with previously reported X-band $^{14,15}N$ 1D and 2D ESEEM spectra. Simulations of X- and S-band spectra provide the hfi and nqi tensors of both nitrogens to SQ_B and a reliable estimation of the N_δ quadrupole coupling constants. This topic is important, as the experimental background for theoretical investigations relies upon an understanding of the relationship between tensor characteristics and the strength (energy) and geometry of H-bonds. Unexpectedly, we find that the nqi and hfi values for the peptide N_p of Gly-L225 lead to suppression of its contribution to the spectrum, despite the near-cancelation condition of N_p at S-band. An explanation for this observation, with full support from DFT calculations, is presented.

MATERIALS AND METHODS

Sample Preparation. Reaction centers used in this study were isolated from a strain of *Rb. sphaeroides* expressing RCs with a histidine tag on the M subunit.[12] Cells were grown under the natural abundance of ^{14}N or in a ^{15}N background using ^{15}N-labeled ammonium sulfate (Cambridge Isotopes). In order to isolate SQ EPR signals, the native high spin Fe^{2+} must be replaced by diamagnetic Zn^{2+}. Procedures for biochemical metal exchange, along with the methods of bacterial cell growth and RC isolation, were as previously described.[10] The SQ_B radical was generated by exposing the RCs to a single 532 nm Nd:YAG laser pulse in the presence of ferrocytochrome *c* (to quickly rereduce the bacteriochlorophyll dimer after charge separation). Upon radical formation, samples were frozen promptly in liquid nitrogen.

S-Band ESEEM. The S-band EPR experiments were performed on an S-band upgraded pulsed EPR ELEXSYS E-580 Bruker spectrometer equipped with an Oxford CF 935 cryostat and ER 4118S-MS5 resonator at 80 K. The frequency of the microwave source was 3.6 GHz, which corresponds to a resonance field of 129 mT for paramagnetic species with a g-factor of ~2. Spectral processing of ESEEM time-domain patterns, including subtraction of the relaxation decay (fitting by polynomials of 3−6 degree), apodization (Hamming window), zero filling, and fast Fourier transformation (FT), was performed using Bruker software WIN-EPR V2.22 Rev. 10. Processed data were then imported into Matlab R2013a to be simulated by EasySpin.[13]

X-Band ESEEM. In this work, we have also used X-band spectra of SQ_B obtained from previously described experiments[10] using ^{14}N and ^{15}N three-pulse ESEEM and the 2D ESEEM technique, HYSCORE (hyperfine sublevel correlation spectroscopy).

Factors Influencing ^{14}N Powder ESEEM Spectra. The ^{14}N nucleus interacting with an unpaired electron spin $S = 1/2$ can produce up to six lines in an ESEEM spectrum. These lines are from transitions between three nuclear energy sublevels in each of the two electron spin manifolds with $m_S = +1/2$ or $-1/2$. Because of differences in orientation dependence, not all transitions contribute equally to the spectra in ESEEM measurements of powder-type samples (such as the frozen RC suspensions used in these experiments). The ESEEM spectrum expected from ^{14}N with a predominantly isotropic hyperfine coupling is governed by the ratio between the effective nuclear frequency in each manifold, $\nu_{ef\pm}$, given by $\nu_{ef\pm} = |\nu_{14N} \pm |A(^{14}N)|/2|$ (where $A(^{14}N)$ is the effective hyperfine coupling), and the quadrupole coupling constant (qcc), $K = e^2Qq/4h$.[14,15]

If $\nu_{ef-}/K \sim 0$, i.e., $\nu_{ef-} \sim 0$ (the situation known as the cancelation condition, because $\nu_{14N} \approx A(^{14}N)/2$), the three nuclear frequencies of the corresponding manifold will be close to the three pure (zero-field) nuclear quadrupole resonance frequencies with ^{14}N transitions

$$\nu_+ = K(3 + \eta) \quad \nu_- = K(3 - \eta) \quad \nu_0 = 2K\eta \tag{1}$$

with the energy levels defined by the principal values of the nqi tensor

$$Q_{max} = 2K \quad Q_{mid} = -K(1 + \eta) \quad Q_{min} = -K(1 - \eta) \tag{2}$$

Both eqs 1 and 2 are completely described by K and the asymmetry parameter η, which ranges in value from 0 to 1. In this case, three narrow peaks at the frequencies given in eq 1 will be present in the powder ESEEM spectrum. These frequencies possess the property $\nu_+ = \nu_- + \nu_0$ and can appear in the spectrum up to a ratio of $\nu_{ef\pm}/K \sim 0.75-1$. However, the intensities of these peaks are also strongly dependent on the time τ chosen between the first two pulses of the ESEEM experiment, so it is important to perform the experiment at multiple values of τ so as to not miss any transitions.

If $\nu_{ef\pm}/K > 1$, only a single line is expected, without pronounced orientation dependence from each corresponding manifold. This line is produced by a transition at the maximum frequency, which is actually a double-quantum transition between the two nuclear outer states with $m_{14N} = -1$ and +1. The frequency of this transition is well described by[14]

$$\nu_{dq\pm} = 2[\nu_{ef\pm}{}^2 + K^2(3 + \eta^2)]^{1/2} \quad (3)$$

Two other single-quantum transitions, involving the central states with $m_{14N} = 0$, usually do not show any resolved peaks because of a significant orientation dependence from the quadrupole interaction.

A more thorough analysis, taking into account the influence of the anisotropic hyperfine interaction, has shown that these simple rules can also be applied to interpret ESEEM spectra when fulfillment of the cancelation condition is considered individually for each principal value of the hfi tensor.[16]

DFT Calculations. The DFT calculations were performed using the B3LYP functional. The EPR-II basis set was used for all atoms except Zn where 6-31g(d) was employed. The model for the calculations was the QM portion of the QM/MM optimized geometry, as described previously.[11] All calculations were performed using the ORCA electronic structure program.[17]

RESULTS AND DISCUSSION

^{14}N and ^{15}N ESEEM Spectra of SQ_B. The interactions of SQ_B with the protein environment in RCs with a natural abundance of nitrogen (^{14}N isotope - 99.63%) and with uniform ^{15}N labeling have been previously studied in detail by X-band pulsed EPR.[10,11] ^{14,15}N HYSCORE spectra clearly resolved the contribution from two nitrogens N1 and N2 carrying unpaired spin density detected through the isotropic hfi coupling. These nitrogens possess different characteristics, i.e., qcc $K = 0.35-0.40$ MHz and isotropic hfi coupling constant $a(^{14}N) \sim 1.5$ MHz for N1 and $K = 0.65-0.75$ MHz and $a(^{14}N) \sim 0.5$ MHz for N2.[10] The values of K characterize the chemical type and electronic configuration of the ^{14}N atoms interacting with SQ_B. For instance, the value of K for N1 most closely corresponds to the protonated nitrogen from an imidazole residue, and that of N2 is typical for a peptide amide nitrogen. On the basis of the X-ray structure and DFT calculations, N1 was identified as N_δ of His-L190 and N2 was assigned as the peptide N_p of Gly-L225 (Figure 1).[10,11]

For both nitrogens, the estimated values of hfi couplings and qcc give a ratio of ν_{ef-}/K in the X-band that deviates by 0.75–1.0 from the cancelation condition ($\nu_{ef-}/K \sim 0$). This is in contrast to SQ_A where two H-bonded nitrogens, from N_δ of His-M219 and the backbone N_p of Ala-M260, possess larger couplings of 2.5 and 1.9 MHz, respectively, with smaller deviations of ν_{ef-}/K from the cancelation condition. In agreement with this conclusion, X-band ESEEM spectra of SQ_A contain well-resolved nqi lines (eq 1) from the His and Ala nitrogens, both identified by parameters K and η as a consequence of the principal values of their nqi tensors.[11] This analysis suggests that the cancelation condition for N1 and N2 in the Q_B site, required for the full determination of the nqi tensor, would be achieved at lower microwave frequencies, yielding a smaller ν_{14N}. In this work, we used S-band with a resonant magnetic field of 128.3 mT for SQ_B, corresponding to $\nu_{14N} = 0.395$ MHz. This decrease in magnetic field strength lowers ν_{ef-}/K (especially for N_p of Gly-L225, to ~0.2), and should promote the appearance of the nqi triplets from both nitrogens in the S-band spectrum.

Figure 2 shows the S-band three-pulse ESEEM spectrum of SQ_B in a stacked representation. The peak at 5.5 MHz corresponds to the matrix ^{1}H feature at the S-band resonant magnetic field. Three "cancelation-like" peaks appearing at 0.55, 0.92, and 1.47 MHz (all ±0.06 MHz) can be attributed to ^{14}N. Formal analysis of these peaks using eq 1 for the nqi triplet gives $K = 0.40$ MHz and $\eta = 0.69$, which are strongly characteristic of the protonated nitrogen of an imidazole residue. According to previous studies, the nqi values of N_δ from histidine hydrogen bonded with the SQs of several quinone sites vary within a narrow interval of $K \sim 0.35-0.43$ MHz and $\eta \sim 0.6-0.8$.[9,18] Under this interpretation, there is seemingly no trace of Gly-L225 N_p in the spectrum, despite the fact that S-band should have brought it even closer to exact cancelation than for His-L190 N_δ. This result is very much unexpected but is accounted for by our simulations of the EPR spectra and DFT calculations as detailed below.

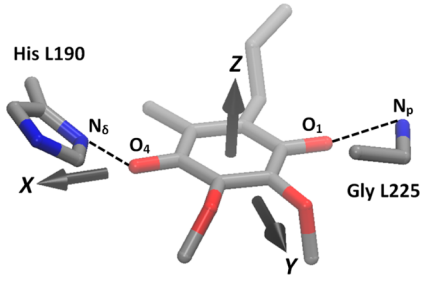

Figure 1. Interaction of SQ_B with its two resolved nitrogen donors His-L190 N_δ and Gly-L225 N_p, which are H-bonded to carbonyl oxygens O_4 and O_1, respectively. The principal axes of the g-tensor are labeled as *X*, *Y*, and *Z*. The g_X axis lies along the line connecting the two oxygen atoms, which carry most of the spin density; the g_Z axis is perpendicular to the molecular plane, and g_Y is perpendicular to both other principal axes. The principal values of the SQ_B g-tensor are $g_X = 2.00626$, $g_Y = 2.00527$, and $g_Z = 2.00213$.[19]

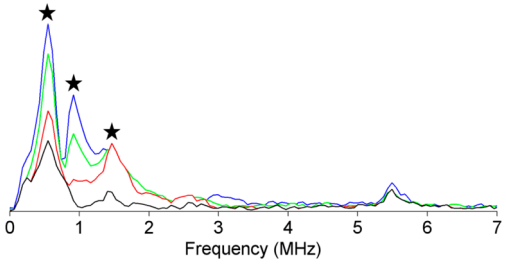

Figure 2. Stacked representation of the two-dimensional set of the S-band three-pulse ESEEM spectra for SQ_B in bacterial RCs. The spectra show the modulus of the Fourier transform along the time T axis at different times, τ. The initial time τ is 192 ns in the blue trace and was increased in steps of 128 ns in successive traces. The nuclear quadrupole resonance frequencies assigned to His-L190 N_δ are marked with stars. A full 3D view is available in the Supporting Information (Figure S6). Experimental parameters: magnetic field 128.3 mT, microwave frequency 3.601 GHz, $\pi/2$ pulse length = 36 ns, temperature 80 K.

^{15}N X-Band HYSCORE and Simulations. The ^{15}N X-band HYSCORE spectrum of SQ_B (Figure 3) consists of a narrow diagonal peak at (ν_{15N}, ν_{15N}) from weakly coupled nitrogens, and two pairs of cross-peaks **1** and **2** from N1 and N2, respectively. They are located symmetrically around the diagonal peak along the antidiagonal, with maxima at (2.53, 0.49) MHz (**1**) and (1.83, 1.16) MHz (**2**) with $a_1(^{15}N) \sim 2.1$ MHz and $a_2(^{15}N) \sim 0.7$ MHz, respectively.[10] Previous analysis based on axial hfi tensor simulations of the individual powder ^{15}N HYSCORE spectra of N1 and N2 showed a significant disagreement in the relative intensity of the cross-peaks **1** and

dx.doi.org/10.1021/jp411023k | J. Phys. Chem. B 2014, 118, 1501–1509

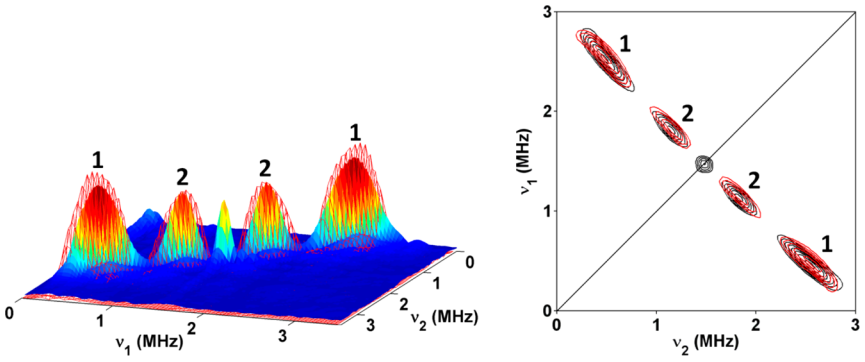

Figure 3. Comparison of experimental and simulated X-band ^{15}N HYSCORE spectra of SQ_B in bacterial RCs in stacked (left) and contour (right) presentation. Peaks labeled as **1** and **2** are assigned to His-L190 N_δ and Gly-L225 N_p, respectively. Simulations are shown in red. Experimental parameters: magnetic field 345.4 mT, time between first and second pulses τ = 136 ns, microwave frequency 9.688 GHz, temperature 80 K. The experimental spectrum is taken from ref 10.

Table 1. ^{14}N Hyperfine Simulation Parameters (^{15}N Data Recalculated for ^{14}N)[a] with DFT Calculated Values in Parentheses

nitrogen	a (MHz)	T (MHz)	δ	Euler angles[b]
N_δ His-L190	|1.3|–|1.4| (1.3)	0.3–0.4 (0.3)	0.5–0.6 (0.0)	[50° 130° −10°] ([0° 110° −10°])
N_p Gly-L225	|0.4| (0.6)	0.2 (0.2)	0 (0.0)	[0° 130° −100°] ([0° 130° −130°])

[a]Principal values of the rhombic hfi tensor: $a + 2T$, $a - T(1 - \delta)$, $a - T(1 + \delta)$; δ ranges from 0 to 1 corresponding to axial and rhombic tensors, respectively. [b]Hfi tensors with δ = 0 (axial) only require the β and γ Euler angles for their full description, so α was set to zero in these cases.

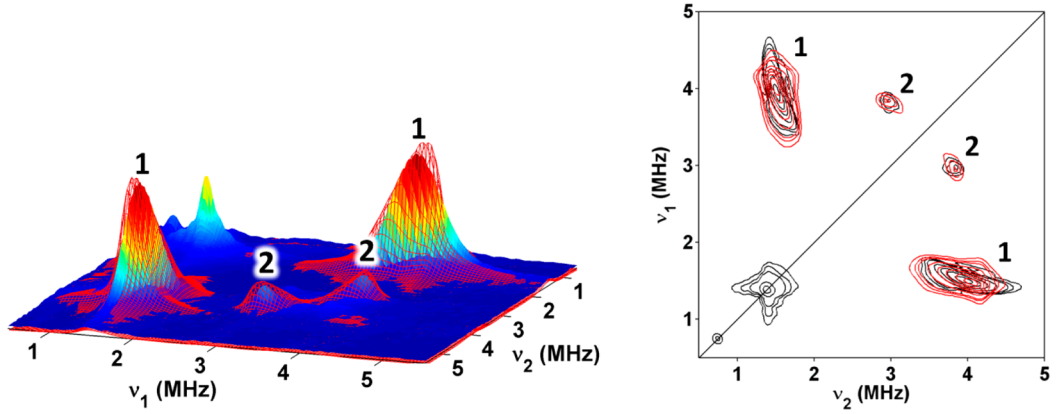

Figure 4. Comparison of experimental and simulated X-band ^{14}N HYSCORE spectra of SQ_B in bacterial RCs in stacked (left) and contour (right) presentation. Peaks labeled as **1** and **2** are assigned to His-L190 N_δ and Gly-L225 N_p, respectively. Simulations are shown in red. Experimental parameters: magnetic field 346.1 mT, time between first and second pulses τ = 136 ns, microwave frequency 9.705 GHz, temperature 80 K. The experimental spectrum is taken from ref 10.

2. Partial improvement was achieved by introducing rhombicity into the hfi.[10] We suggested that further improvement would necessitate simulating N1 and N2 together, with both hfi tensors defined in the same coordinate system.

Simulations of the ESEEM spectra were performed in the g-tensor coordinate system of SQ_B. The principal axes of the g-tensor (X, Y, Z) with respect to the molecular structure of the quinone have been defined by single-crystal EPR experiments for SQ_A,[19] and are shown in Figure 1. The simulated peak maxima were in strong agreement with the experimental peak positions (Table S1, Supporting Information). The orientations of the hfi and nqi tensor principal axes for N_δ of His-L190 and N_p of Gly-L225 were defined relative to the g-tensor axes with Euler angles (α, β, and γ) in accordance with the EasySpin program (http://www.easyspin.org)[13] and as described in the Supporting Information.

Comparison of the experimental and simulated ^{15}N HYSCORE spectra for SQ_B is shown in Figure 3. All parameters were recalculated for ^{14}N and are listed in Table 1. Simulations were found to be relatively insensitive to Euler angles, especially for α and γ. Therefore, Euler angles were determined with better confidence from the ^{14}N spectra. The weak dependence between the Euler angles and the resulting ^{15}N spectrum is likely due to the low level of hfi anisotropy.

The choice of hfi tensor principal values, on the other hand, had a large impact on the resulting ^{15}N HYSCORE simulation. Initial parameters for the tensors were taken from the previous analysis of contour line shapes and separate simulations for N1 and N2.[10] The correct intensity ratio of the two features could be obtained when N_p of Gly-L225 was assigned an axial hfi tensor and N_δ of His-L190 with a more rhombic tensor. Simulation parameters for the spectrum giving the optimum relative intensity for cross-peaks N1 and N2 and a reasonable line shape in comparison with the experimental spectrum are listed in Table 1. Euler angles included in Table 1 were determined from the ^{14}N spectra as discussed below.

dx.doi.org/10.1021/jp411023k | J. Phys. Chem. B 2014, 118, 1501–1509

^{14}N X- and S-Band ESEEM and Simulations. The X-band ^{14}N HYSCORE spectrum of SQ_B (Figure 4) exhibits intense and extended cross-ridges **1** possessing a maximum at (3.96, 1.51) MHz and a second pair of cross-peaks **2** of circular shape with smaller intensity and a maximum at (3.86, 2.98) MHz.[10] Simulations produced reasonable agreement with these experimental maxima (Table S1, Supporting Information). Previous analysis has shown that cross-peaks **1** and **2** correlate double-quantum (dq) transitions from opposite manifolds, i.e., ν_{dq+} and ν_{dq-}, for N1 and N2, respectively. The spectrum does not resolve any other cross-peaks. A significant orientation dependence of the single-quantum transitions very likely explains the lack of additional features. The corresponding X-band three-pulse ESEEM spectrum (Figure 5) also shows dq features as an intense line at 1.5 MHz, a weak peak at 2.9 MHz, and a broad feature around 3.8 MHz. At lower frequency, there is a peak at ~0.3 MHz and a feature around 0.7 MHz that appears to contain overlapping lines. The shapes of these peaks are affected by the procedures preceding the FT analysis, particularly by the degree of polynomial used for extraction of the relaxation decay. Accordingly, our original three-pulse ESEEM spectrum[10] has been reanalyzed in this work to minimize suppression of the low frequency peaks.

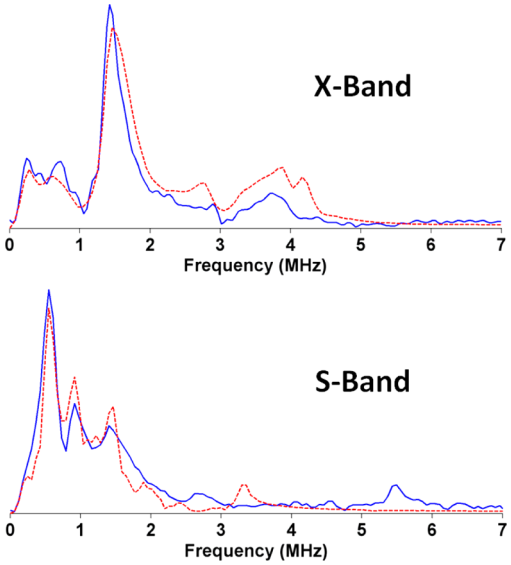

Figure 5. Comparison of experimental (blue) and simulated (red) X- (top) and S- (bottom) band ^{14}N three-pulse ESEEM spectra of SQ_B in bacterial RCs. Experimental parameters: X-band, magnetic field 346.1 mT, microwave frequency 9.705 GHz, time τ = 100 ns; S-band, magnetic field 128.3 mT, microwave frequency 3.601 GHz, time τ = 320 ns.

^{14}N 1D and 2D ESEEM were simulated with full hfi and nqi tensors for both nuclei. It is well established that the principal directions of the nqi tensor for the N_δ imine nitrogen are associated with the molecular axes of the imidazole residue (Figures 1 and S1, Supporting Information).[20−23] These axes are retained if this nitrogen is coordinated to a metal or H-bonded, and thus can be used for the characterization of the imidazole orientation. This approach has been verified by several experiments showing that the principal directions of the nqi tensor determined by magnetic resonance techniques provide the correct description of the ligand geometry by comparison with X-ray crystal structures.[20−22,24]

The principal values of the nqi tensor are $|Q_{max}| = 2K$, $|Q_{mid}| = K(1 + \eta)$, and $|Q_{min}| = K(1 - \eta)$. The orientation of the principal axes of the nqi tensor with respect to the molecular frame has been theoretically analyzed for protonated nitrogens of imidazole and peptide bonds in several different systems. For a hydrogen bond between SQ_B and N_δ of His-L190, an appropriate calculation of the nqi tensor is that of *N*-methylimidazole H-bonded to a semiquinone.[23] According to this study, the Q_{min} direction points along the N−H bond (x axis), the Q_{max} direction is perpendicular to the imidazole plane (z axis), and Q_{mid} is in the imidazole plane, perpendicular to the N−H bond (y axis) (Figure S1, Supporting Information). However, especially short H-bonds (as indicated by a high η value) resulted in an interchange of the Q_{max} and Q_{mid} principal directions. Under this condition, Q_{max} lies in the imidazole plane. This orientation of Q_{max} has been observed experimentally for the $N_\delta H$ (K = 0.35 MHz, η = 0.66) in Cu(II)-doped single crystals of L-histidine hydrochloride[22] and in L-histidine monochloride monohydrate (K = 0.32 MHz, η = 0.946).[20] In contrast, Q_{max} for $N_\varepsilon H$ (K = 0.366 MHz, η = 0.268) in L-histidine monochloride monohydrate was found to be normal to the imidazole plane.[18] The nqi diversity observed in L-histidine monochloride was explained by differences in intermolecular hydrogen bonding at each nitrogen. The H-bond length H···O 1.58 Å for the N_δ is significantly shorter than 1.94 Å for the N_ε.[20] This behavior is in agreement with the calculations of Fritscher.[23] In reaction centers, the length of the O4−HN$_\delta$ His-L190 H-bond in the optimized structure of SQ_B is 1.58 Å, suggesting a strong hydrogen bond, as supported by the hfi tensor of the H-bonding proton.[11] Additionally, the characteristics of the nqi tensor of $N_\delta H$ in Cu(II)-doped single crystals of L-histidine hydrochloride[22] are very close to the values observed for the histidine nitrogen H-bonded with SQ_B. If one accepts that this system mimics well the His-L190 coordinated with Zn(II) and H-bonded with O4 of SQ_B, then Q_{max} for N_δ is expected to have a stable value of the order ~0.70−0.86 MHz and a preferred direction along the y molecular axis in the imidazole plane. Our DFT calculations of SQ_B were in excellent agreement with this assignment of the nqi tensor orientation, with the calculated principal components having Q_{min} approximately along the x molecular axis, Q_{mid} perpendicular to the imidazole ring (z axis), and Q_{max} in-plane with the imidazole (y axis) (Table 2 and Figures S2 and S3, Supporting Information). However, we note that when simulations were performed with Q_{max} perpendicular to the imidazole plane (Euler angles [170° 30° −10°]) accompanied by a small adjustment of the His-L190 hfi tensor orientation (Euler angles [60° 110° −10°]) but all other simulation parameters unchanged, an equally good fit to the experimental data was achieved. Therefore, the possibility that Q_{max} takes on

Table 2. ^{14}N X- and S-Band Quadrupole Simulation Parameters with DFT Calculated Values in Parentheses

nitrogen	K (MHz)	η	Euler angles
N_δ His-L190	|0.38|−|0.39| (0.40)	0.69 (0.94)	[−120° 90° −100°] ([−120° 80° −100°])
N_p Gly-L225	|0.74| (−0.98)	0.45 (0.43)	[−120° 60° −160°] ([−160° 60° −160°])

dx.doi.org/10.1021/jp411023k | J. Phys. Chem. B 2014, 118, 1501−1509

a perpendicular orientation relative to the imidazole plane cannot be completely eliminated.

The amide nitrogen in free peptides, such as in metal complexes of diglycine, which H-bonds to the inorganic sulfur atoms of iron−sulfur clusters,[25−31] has a narrow range of qcc (K = 0.75−0.85 MHz) determined by the electronic structure and the geometry of the planar peptide group. This coupling constant is only slightly perturbed by hydrogen bonding, as has been confirmed by calculations of the nqi tensor.[28,32,33] From these calculations, it was found that the Q_{max} principal direction is normal to the local peptide plane, the Q_{mid} direction almost coincides with the C(O)−N(H) bond, and Q_{min} points about 30° off of the N−H bond. Our DFT calculations were again in good agreement with this assigned orientation for the peptide N_p Gly-L225 nqi tensor axes (Table 2 and Figures S2 and S3, Supporting Information). Reported qcc's of peptide nitrogens hydrogen bonded with semiquinones of different quinone sites are also within the interval indicated above.[34−36]

In the crystal structure 1DV3, the main population of Q_B is in the proximal position. Therefore, coordinates from this crystal structure were combined with the theoretically predicted orientations of the principal directions of the nqi tensor, and the corresponding Euler angles relative to the g-tensor axes for His-L190 N_δ and Gly-L225 N_p were calculated and fixed in the EPR simulations. The initial nqi parameters for His-L190 N_δ were obtained from the S-band spectrum for N_δ as K = 0.40 MHz and η = 0.69. For Gly-L225 N_p, our ^{14}N ESEEM data for N_p of Ala-M260 H-bonded with SQ_A were used as initial parameters, i.e., K = 0.77 MHz and η = 0.63 MHz, following from the nqi triplet: 1.0, 1.8, 2.8 MHz.[11] No assumptions were made about the Euler angles defining the orientations of the axes for hfi tensors.

To provide justification for the assignment of the lines in the S-band spectra, simulations were done simultaneously along with ^{14}N X-band three-pulse and ^{14,15}N HYSCORE spectra. Therefore, optimization involved judging the parameters' ability to reproduce all four spectra, as opposed to just one. Once an optimal set was found, a tolerance window of 0.1 MHz was given to the His-L190 N_δ hfi and nqi coupling constant parameters (Tables 1 and 2). This small degree of flexibility reflects the error underlying the various assumptions built into the simulations (e.g., ideal pulse shape and full excitation of the SQ line width). Nevertheless, only minor adjustments to the initial hfi and nqi tensors within the allotted tolerance window were needed to obtain very satisfactory simulations, and the optimized hfi Euler angles were in excellent agreement with the DFT calculated values (Tables 1 and 2, Figures S4 and S5, Supporting Information). All of the ^{14}N simulations are shown in red in Figures 3, 4, and 5, overlaying the experimental spectra. In addition, we have compared the three-pulse S-band simulations performed separately on N_δ from His-L190 and on N_p of Gly-L225 to show N_p makes only a very small contribution to the total S-band spectrum (Figure 6).

An Explanation for the Suppression of the N_p Contribution to the S-Band Spectrum. The peculiarities of the S-band spectrum cannot be explained qualitatively using the simple approach based on the approximation of a purely isotropic hfi. Analysis of the simulation results from Tables 1 and 2 allows us to conclude that this approximation is not fully satisfied, especially in the case of Gly-L225 N_p. Quantitatively, variation of the hfi coupling in changing from $a + 2T$ to $a - T$ (under an axial approximation) can be characterized by its range $3T$, which in our case is comparable with the ^{14}N Zeeman

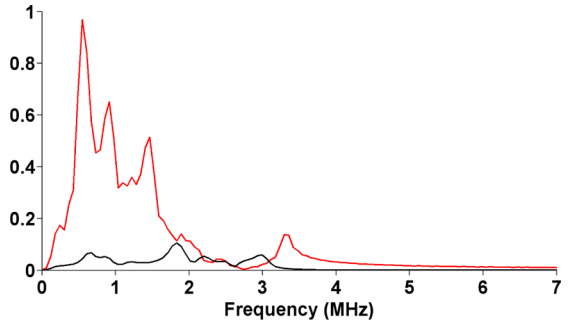

Figure 6. Comparison between separate ^{14}N S-band ESEEM simulations done for His-L190 N_δ (red) and Gly-L225 N_P (black). With the given parameters (Tables 1 and 2), Gly-L225 N_p makes a minimal contribution to the overall spectral intensity.

frequency in X-band or even exceeding ν_{14N} in S-band for both nitrogens (Table 3). In this case, the peculiarities of the spectral features can be understood by considering the fulfillment of the condition $\nu_{ef\pm}/K < 0.7-1.0$ for different principal values of hfi tensors (shown in bold in Table 3).[16]

This analysis is summarized in Table 3. One can see that for N_δ His-L190 at S-band the two smallest principal values A_1 and A_2 of the hfi tensor give ν_{ef-}/K values of 0.16 and 0.55, respectively. These values of ν_{ef-}/K, which comprise the perpendicular component of the hfi tensor under the axial approximation, justify the appearance of the nqi triplet in the S-band spectra despite the fact that a ratio of ν_{ef-}/K = 0.8 for an isotropic coupling $a(^{14}N)$ = 1.4 MHz of this nitrogen might suggest a distortion of this triplet. The set of conformations in the (A_1, A_2) plane produces the triplet nqi spectrum. The spread of ν_{ef-}/K leads to the observed line broadening surrounding the peak maxima. Nevertheless, the peak maxima satisfy the nqi condition well (eq 1). Simulation of the X- and S-band spectra led to only a very minor correction of the K value estimated from the experimental spectrum (Table 2).

Similarly to His-L190 N_δ, the transition from the X- to S-band shifts ν_{ef-}/K for all principal values of Gly-L225 N_p toward a range appropriate for the observation of the nqi triplet. However, the S-band spectra do not exhibit lines typical for nqi frequencies of N_p. An explanation for this comes from previous computational and theoretical analyses showing that the amplitudes of the nqi peaks also vary with ν_{14N}/K. At a low ν_{14N}/K ratio, the energy levels in both manifolds approach each other and ESEEM vanishes at about $\nu_{14N}/K < 0.3$.[14] Finally, the condition of exact cancelation is not sufficient to produce intense ESEEM peaks, with an additional requirement being that $A(^{14}N) \geq K$.[15] If $A(^{14}N) < K$, then the ESEEM intensity is expected to be weak even at exact cancelation.

Transition from X- to S-band decreases the ν_{14N}/K ratio by almost 3-fold (2.68), giving $\nu_{14N}/K \approx 0.5$ for N_p. The simulated spectra (Figure 6) show substantial suppression of spectral intensity from N_p in agreement with the theoretical considerations provided above. This suggests that the intensity of the spectrum would increase with an increase of the isotropic coupling. Figure 7 shows that increasing the isotropic coupling 2−3-fold, without changing any other parameters, significantly increases the spectral intensity as expected.

The S-Band Defined nqi Tensor of His-L190 N_δ. Previous analyses of ESEEM[37a] and nuclear quadrupole resonance[37b] measurements determined the values of e^2qQ/h and η for imidazole $^{14}N_\delta$ in different compounds to be sensitive to hydrogen-bond formation through a change in electron

dx.doi.org/10.1021/jp411023k | J. Phys. Chem. B 2014, 118, 1501−1509

Table 3. Comparative Characteristics of Magnetic Interactions for N_δ His-L190 and N_p Gly-L225 in X- and S-Band ESEEM Experiments

nitrogen	N_δ His-L190						N_p Gly-L225					
K (MHz)	0.38−0.39						0.74					
band	X-band			S-band			X-band			S-band		
ν_{14N} (MHz)	1.06			0.395			1.06			0.395		
ν_{14N}/K	2.72−2.79			1.01−1.04			1.43			0.53		
A_1, A_2, A_3[a] (MHz)	0.9	1.2	2.0	0.9	1.2	2.0	0.2	0.2	0.9	0.2	0.2	0.9
ν_{ef-}	0.61	0.46	0.06	0.06	0.21	0.61	0.96	0.96	0.61	0.30	0.30	0.06
ν_{ef-}/K	1.58	1.19	0.16	**0.16**	**0.55**	**1.58**	1.30	1.30	0.82	**0.41**	**0.41**	**0.08**
ν_{ef+}	1.51	1.66	2.06	0.85	1.00	1.40	1.16	1.16	1.51	0.50	0.50	0.85
ν_{ef+}/K	3.92	4.31	5.35	2.21	2.60	3.64	1.57	1.57	2.04	0.68	0.68	1.15

[a]Principal values of the rhombic hfi tensor: $a + 2T$, $a - T(1 - \delta)$, $a - T(1 + \delta)$.

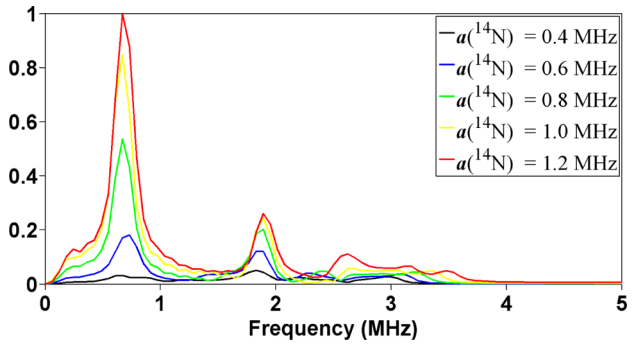

Figure 7. Simulated three-pulse S-band ESEEM spectra of Gly-L225 N_p as a function of increasing $a(^{14}N)$ in steps of 0.2 MHz. All other parameters are fixed to the values listed in Tables 1 and 2.

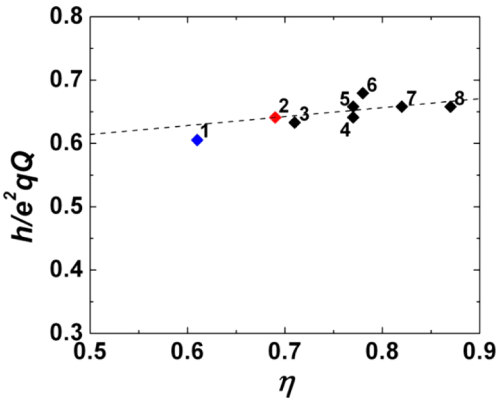

Figure 8. Values of h/e^2qQ and η for histidine $^{14}N_\delta$ interacting with SQ_A in bacterial and PSII RCs (black) and SQ_B in bacterial RCs reported by Lendzian et al. (ref 40) (blue) and this work (red). The linear fit (dashed line) was performed for only the points corresponding to SQ_A. (1) Q_B^- in *Rhodobacter sphaeroides* (ref 40), (2) Q_B^- in *Rhodobacter sphaeroides* (this work), (3) Q_A^- in high-pH-treated PSII pH 9.2 (ref 35), (4) Q_A^- in CN-treated PSII pH 5.5 (ref 35), (5) Q_A^- in $LiClO_4$-treated PSII pH 6.0 (ref 39), (6) Q_A^- in high-pH-treated PSII pH 5.0 (ref 35), (7) Q_A^- in *Rhodobacter sphaeroides* (ref 34), (8) Q_A^- in *Rhodopseudomonas viridis* (ref 38, the nqi tensor was reported incorrectly in the table of this reference: we have reanalyzed their spectra on the basis of their assigned peak positions).

occupancy of the nitrogen orbitals.[37] It was concluded that a stronger H-bond would lower the p_π orbital spin population and increase the N−H orbital population, subsequently reducing the e^2qQ/h value and increasing η. Empirically, this influence can be described with good accuracy by the linear dependence between h/e^2qQ and η. Figure 8 shows h/e^2qQ and η values for histidine $^{14}N_\delta$ interacting with SQ_A[34,35,38,39] in bacterial reaction centers and in photosystem II. The points in Figure 8 are clustered in the region with $\eta \geq 0.7$. Also shown is the point (blue) corresponding to the previously reported SQ_B $^{14}N_\delta$ nqi tensor values (e^2qQ/h = 1.65 MHz and η = 0.61);[40] it is substantially shifted to a lower η, away from the "Q_A area", suggesting the formation of a significantly weaker hydrogen bond. However, this estimation of the $^{14}N_\delta$ nqi tensor was based on the analysis of an X-band three-pulse ESEEM spectrum not satisfying the cancelation condition, and therefore prone to distortion of the peak maxima (see discussion in ref 10). The characteristics of the nqi tensor reported in this work move the Q_B point (red) to within the range of the Q_A points; this is more consistent with the similar value of the anisotropic hyperfine tensor component $T \sim 5.2$ MHz for the proton involved in the H-bond between N_δ and SQ_B, which is similar to the complementary $T \sim 5.4$ MHz for the Q_A site in RCs from *Rb. sphaeroides*.

CONCLUSION

S-band ESEEM was performed on SQ_B in bacterial RCs with the aim of determining the principal values of the nqi tensor for the hydrogen bond donors N_δ of His-L190 and N_p of Gly-L225. The resulting three-pulse spectrum showed a visible contribution only from N_δ of His-L190, despite the shift of the ^{14}N Zeeman frequency toward a region expected to nearly satisfy the cancelation condition for both nitrogens, as predicted from the data obtained in previous X-band experiments. Simultaneous simulation of 1D and 2D X-band and S-band ESEEM spectra confirmed this experimental result. Analysis of the simulation parameters allowed us to conclude that the N_p contribution to the S-band spectrum is suppressed as a result of the typically large qcc of N_p in combination with its relatively small isotropic hyperfine coupling and comparable hfi tensor anisotropy. ESEEM intensity vanishes under these conditions, despite even better fulfillment of the cancelation condition for N_p than for N_δ of His-L190. Nevertheless, simulations successfully reproduced the experimental X-band data for N_p, and were well supported by DFT calculations.

The observed triplet of lines for His-L190 corresponding to the zero-field nqi frequencies (eq 1) was simulated as qcc e^2qQ/h = 1.54 ± 0.02 MHz with an asymmetry parameter η = 0.69 and defines the principal values (eq 2) of the nqi tensor for N_δ of His-L190. These data significantly improve upon a previous analysis not performed under the cancelation condition.[40] Our results show the strength and applicability of S-band for obtaining accurate nqi parameters for weakly coupled nuclei.

dx.doi.org/10.1021/jp411023k | J. Phys. Chem. B 2014, 118, 1501−1509

While estimation of the hfi tensor alignment to the molecular frame is best done by EPR on single crystals, it is often very difficult to obtain single crystal radical samples for a protein of interest. In this study, we show that simultaneous simulation of the ^{14}N S- and X-band three-pulse spectra and ^{14,15}N HYSCORE spectra (with a tolerance window of 0.1 MHz) produces remarkable agreement with the DFT calculated tensor orientations. The success of DFT to reproduce the experimentally determined hfi and nqi tensors highlights the reliability of modern DFT for predicting EPR parameters. Additionally, our findings, taken as a whole, show promise for future ESEEM determinations of Euler angles for nuclei not suitable for high-frequency ENDOR measurements[41,42] (such as weakly coupled nitrogens) or in a spin system not readily crystallizable in the radical state.

■ ASSOCIATED CONTENT

Supporting Information

Euler angle definitions; Table S1 - simulated and experimental peak maxima of HYSCORE; Figures S1−S5 - calculated and experimental g and nqi tensors relative to the molecular frame of SQ_B. This material is available free of charge via the Internet at http://pubs.acs.org.

■ AUTHOR INFORMATION

Corresponding Authors

*E-mail: dikanov@illinois.edu. Phone: (217) 300-2209.
*E-mail: cwraight@life.illinois.edu. Phone: (217) 333-3245.
*E-mail: patrick.omalley@manchester.ac.uk. Phone: 00441612004536.

Author Contributions

The manuscript was written through contributions of all authors. All authors have given approval to the final version of the manuscript.

Notes

The authors declare no competing financial interest.

■ ACKNOWLEDGMENTS

This research was supported by the DE-FG02-08ER15960 Grant from Chemical Sciences, Geosciences and Biosciences Division, Office of Basic Energy Sciences, Office of Sciences, U.S. Department of Energy and NIH Grant GM062954 (S.A.D.), NSF Grant MCB-0818121 (C.A.W.), and NCRR/NIH Grant S10-RR15878 and S10-RR025438 for pulsed EPR instrumentation. A.T.T. gratefully acknowledges support as a NIH trainee of the Molecular Biophysics Training Program (5T32-GM008276). P.J.O'M. acknowledges the use of computer resources granted by the EPSRC UK national service for computational chemistry software (NSCCS).

■ REFERENCES

(1) Heathcote, P.; Fyfe, P. K.; Jones, M. R. Reaction Centers: The Structure and Evolution of Biological Solar Power. *Trends Biochem. Sci.* **2002**, *27*, 79−86.

(2) Blankenship, R. *Molecular Mechanisms of Photosynthesis*; Blackwell Science, Ltd: London, 2002.

(3) Wraight, C. A. Proton and Electron Transfer in the Acceptor Quinone Complex of Photosynthetic Reaction Centers from *Rhodobacter sphaeroides*. *Front. Biosci.* **2004**, *9*, 309−337.

(4) Okamura, M. Y.; Paddock, M. L.; Graige, M. S.; Feher, G. Proton and Electron Transfer in Bacterial Reaction Centers. *Biochim. Biophys. Acta* **2000**, *1458*, 148−163.

(5) Wraight, C. A.; Gunner, M. R. The Acceptor Quinones of Purple Photosynthetic Bacteria − Structure and Spectroscopy. In *The Purple Phototrophic Bacteria*; Hunter, C. N., Daldal, F., Thurnauer, M. C., Beatty, J. T., Eds.; Springer: Dordrecht, The Netherlands, 2009; p 379.

(6) Stowell, M. H. B.; McPhillips, T. M.; Rees, D. C.; Solitis, S. M.; Abresch, E.; Feher, G. Light-Induced Structural Changes in Photosynthetic Reaction Center: Implications for Mechanism of Electron-Proton Transfer. *Science* **1997**, *276*, 812−816.

(7) Koepke, J.; Krammer, E. M.; Klingen, A. R.; Sebban, P.; Ullmann, G. M.; Fritzsch, G. pH Modulates the Quinone Position in the Photosynthetic Reaction Center from *Rhodobacter sphaeroides* in the Neutral and Charge Separated States. *J. Mol. Biol.* **2007**, *371*, 396−409.

(8) Lubitz, W.; Feher, G. The Primary and Secondary Acceptors in Bacterial Photosynthesis III. Characterization of the Quinone Radicals $Q_A^{-\bullet}$ and $Q_B^{-\bullet}$ by EPR and ENDOR. *Appl. Magn. Reson.* **1999**, *17*, 1−48.

(9) Dikanov, S. A. Resolving Protein-Semiquinone Interactions by Two-Dimensional ESEEM Spectroscopy. *Electron Paramagn. Resonan.* **2013**, *23*, 103−179.

(10) Martin, E.; Samoilova, R. I.; Narasimhulu, K. V.; Wraight, C. A.; Dikanov, S. A. Hydrogen Bonds between Nitrogen Donors and the Semiquinone in the Q_B site of Bacterial Reaction Centers. *J. Am. Chem. Soc.* **2010**, *132*, 11671−11677.

(11) Martin, E.; Samoilova, R. I.; Narasimhulu, K. V.; Lin, T. J.; O'Malley, P. J.; Wraight, C. A.; Dikanov, S. A. Hydrogen Bonding and Spin Density Distribution in the Q_B Semiquinone of Bacterial Reaction Centers and Comparison with the Q_A Site. *J. Am. Chem. Soc.* **2011**, *133*, 5525−5537.

(12) Goldsmith, J. O.; Boxer, S. G. Rapid Isolation of Bacterial Photosynthetic Reaction Center with an Engineered Poly-Histidine Tag. *Biochim. Biophys. Acta* **1996**, *1276*, 171−175.

(13) Stoll, S.; Britt, R. D. General and Efficient Simulation of Pulse EPR Spectra. *Phys. Chem. Chem. Phys.* **2009**, *11*, 6614−6625.

(14) Dikanov, S. A.; Tsvetkov, Yu. D.; Bowman, M. K.; Astashkin, A. V. Parameters of Quadrupole Coupling of ^{14}N Nuclei of Chlorophyll *a* Cations Determined by Electron Spin Echo Method. *Chem. Phys. Lett.* **1982**, *90*, 149−153.

(15) Flanagan, H.; Singel, D. J. Analysis of ^{14}N ESEEM Patterns of Randomly Oriented Solids. *J. Chem. Phys.* **1987**, *87*, 5606−5616.

(16) Benetis, N. P.; Dikanov, S. A. Influence of the Anisotropic Hyperfine Interaction on the ^{14}N ENDOR and the ESEEM Orientation-Disordered Spectra. *J. Magn. Reson.* **2005**, *175*, 124−145.

(17) Neese, F. The ORCA Program System. *Wiley Interdiscip. Rev.: Comput. Mol. Sci.* **2012**, *2*, 73−78.

(18) Dikanov, S. A.; Holland, J. T.; Endeward, B.; Kolling, D. R. J.; Samoilova, R. I.; Prisner, Th. F.; Crofts, A. R. Hydrogen Bonds between Nitrogen Donors and the Semiquinone in the Q_i-Site of the bc_1 Complex. *J. Biol. Chem.* **2007**, *282*, 25831−25841 (see Table 2 in this reference).

(19) Isaacson, R. A.; Lendzian, F.; Abresch, E. C.; Lubitz, W.; Feher, G. Electronic Structure of Q_A^- in Reaction Centers from *Rhodobacter sphaeroides*. I. Electron Paramagnetic Resonance in Single Crystals. *Biophys. J.* **1995**, *69*, 311−322.

(20) McDowell, C. A.; Naito, A.; Sastry, D. L.; Takegoshi, K. Determination of the ^{14}N Quadrupole Coupling Tensor in a Single Crystal of *l*-Histidine Hydrochloride Monohydrate by NMR Spectroscopy. *J. Magn. Reson.* **1986**, *69*, 283−292.

(21) McDowell, C. A.; Naito, A.; Sastry, D. L.; Cui, Y. U.; Sha, K.; Yu, S. X. Ligand ENDOR Study of Cu(II)-Doped *l*-Histidine Deuterochloride Monodeuterohydrate Single Crystals at 4.2 K. *J. Mol. Struct.* **1989**, *195*, 361−381.

(22) Colaneri, M. J.; Peisach, J. An Electron Spin-Echo Envelope Modulation Study of Cu(II)-Doped Single Crystals of L-Histidine Hydrochloride Monohydrate. *J. Am. Chem. Soc.* **1992**, *114*, 5335−5341.

(23) Fritscher, J. Influence of Hydrogen Bond Geometry on Quadrupole Coupling Parameters: A Theoretical Study of Imidazole−Water and Imidazole−Semiquinone Complexes. *Phys. Chem. Chem. Phys.* **2004**, *6*, 4950−4956.

(24) Reijerse, E. J.; Tyryshkin, A. M.; Dikanov, S. A. Complete Determination of Nitrogen Quadrupole and Hyperfine Tensors in an Oxovanadium Complex by Simultaneous Fitting of Multifrequency ESEEM Powder Spectra. *J. Magn. Reson.* **1998**, *131*, 295−309.
(25) Edmonds, D. T.; Speight, P. A. Nitrogen Quadrupole Resonance in Amino Acids. *Phys. Lett. A* **1971**, *34*, 325−326.
(26) Blinc, R.; Mali, M.; Osredkar, R.; Seliger, J.; Ehrenberg, L. ^{14}N Quadrupole Resonance in Polyglycine. *Chem. Phys. Lett.* **1974**, *28*, 158−159.
(27) Ashby, C. I.; Paton, W. F.; Brown, T. L. Nitrogen-14 Nuclear Quadrupole Resonance Spectra of the Coordinated Amino Group and of Coordinated Imidazole. Crystal and Molecular Structures of Chloroglycylglycinato(imidazole)cadmium. *J. Am. Chem. Soc.* **1980**, *102*, 2990−2998.
(28) Rabbani, S. R.; Edmonds, D. T.; Gosling, P.; Palmer, M. H. Measurement of the ^{14}N Quadrupole Coupling Constants in Glycine, Diglycine, Triglycine, and Tetraglycine and a Comparison with Calculation. *J. Magn. Reson.* **1987**, *72*, 230−237.
(29) Dikanov, S. A.; Tyryshkin, A. M.; Felli, I.; Reijerse, E. J.; Huettermann, J. C-band ESEEM of Strongly Coupled Peptide Nitrogens in Reduced Two-Iron Ferredoxin. *J. Magn. Reson., Ser. B* **1995**, *108*, 99−102.
(30) Mims, W. B.; Peisach, J. ESEEM and LEFE of Metalloproteins and Model Compounds. In *Advanced EPR: Applications in Biology and Biochemistry*; Hoff, A. J., Ed.; Elsevier Science Publishers B.V.: Amsterdam, The Netherlands, 1989; pp 1−57.
(31) Dikanov, S. A.; Kolling, D. R. J.; Endeward, B.; Samoilova, R. I.; Prisner, T. F.; Nair, S. K.; Crofts, A. R. Identification of Hydrogen Bonds to the Rieske Cluster through the Weakly Coupled Nitrogens Detected by Electron Spin Echo Envelope Modulation Spectroscopy. *J. Biol. Chem.* **2006**, *281*, 27416−27425.
(32) Palmer, M. H. ^{14}N Nuclear Quadrupole Coupling in Glycylglycine and Related Peptides. *Z. Naturforsch.* **1984**, *39B*, 1108−1111.
(33) Elmi, F.; Hadipour, N. L. A Study on the Intermolecular Hydrogen Bonds of α-Glycylglycine in its Actual Crystalline Phase using *ab initio* Calculated ^{14}N and ^{2}H Nuclear Quadrupole Coupling Constants. *J. Phys. Chem. A* **2005**, *109*, 1729−1733.
(34) Spoyalov, A. P.; Hulsebosch, R. J.; Shochat, S.; Gast, P.; Hoff, A. J. Evidence that Ala M260 is Hydrogen-Bonded to the Reduced Primary Acceptor Quinone Q_A^- in Reaction Centers of *Rb. sphaeroides*. *Chem. Phys. Lett.* **1996**, *263*, 715−720.
(35) Deligiannakis, Y.; Hanley, J.; Rutherford, A. W. 1D- and 2D-ESEEM Study of the Semiquinone Radical Q_A^- of Photosystem II. *J. Am. Chem. Soc.* **1999**, *121*, 7653−7664.
(36) Chatterjee, R.; Milikisiyants, S.; Coates, C. S.; Lakshmi, K. V. High-Resolution Two-Dimensional ^{1}H and ^{14}N Hyperfine Sublevel Correlation Spectroscopy of the Primary Quinone of Photosystem II. *Biochemistry* **2011**, *50*, 491−501.
(37) (a) Jiang, F.; McCracken, J.; Peisach, J. Nuclear Quadrupole Interactions in Cu(II)-Diethylenetriamine-Substituted Imidazole Complexes and in Cu(II) Proteins. *J. Am. Chem. Soc.* **1990**, *112*, 9035−9044. (b) Hiesh, Y. N.; Rubenacker, G. V.; Cheng, C. P.; Brown, T. L. Nitrogen-14 Nuclear Quadrupole Resonance Spectra of Coordinated Pyridine. *J. Am. Chem. Soc.* **1977**, *99*, 1384−1389.
(38) Gardiner, A. T.; Zech, S. G.; MacMillan, F.; Käss, H.; Bittl, R.; Schlodder, E.; Lendzian, F.; Lubitz, W. Electron Paramagnetic Studies of Zinc-Substituted Reaction Centers from *Rhodopseudomonas viridis*. *Biochemistry* **1999**, *38*, 11773−11787.
(39) Astashkin, A. V.; Hara, H.; Kuroiwa, S.; Kawamori, A.; Akabori, K. A Comparative Electron Spin Echo Envelope Modulation Study of the Primary Electron Acceptor Quinone in Zn-Substituted and Cyanide-Treated Preparations of Photosystem II. *J. Chem. Phys.* **1998**, *108*, 10143−10151.
(40) Lendzian, F.; Rautter, J.; Käß, H.; Gardiner, A.; Lubitz, W. ENDOR and Pulsed EPR Studies of Photosynthetic Reaction Centers: Protein Cofactor Interactions. *Ber. Bunsen-Ges. Phys. Chem.* **1996**, *100*, 2036−2040.
(41) Flores, M.; Isaacson, R. A.; Calvo, R.; Feher, G.; Lubitz, W. Probing Hydrogen Bonding to Quinone Anion Radicals by ^{1}H and ^{2}H ENDOR Spectroscopy at 35 GHz. *Chem. Phys.* **2003**, *294*, 401−413.
(42) Schnegg, A.; Dubinskii, A. A.; Fuchs, M. R.; Grishin, Y. A.; Kirilina, E. P.; Lubitz, W.; Plato, M.; Savitsky, A.; Möbius, K.; High-Field, E. P. R. ENDOR and ELDOR on Bacterial Photosynthetic Reaction Centers. *Appl. Magn. Reson.* **2007**, *31*, 59−98.